

Regeneration of *Bombyx mori* silk by electrospinning. Part 3: characterization of electrospun nonwoven mat

Jonathan Ayutsede^a, Milind Gandhi^b, Sachiko Sukigara^c, Michael Micklus^a, Hung-En Chen^d,
Frank Ko^{a,*}

^aFibrous Materials Laboratory, Department of Materials Science and Engineering, Drexel University, 31st and Market Street, Philadelphia, PA 19104, USA

^bSchool of Biomedical Engineering, Sciences and Health System, Drexel University, Philadelphia, PA 19104, USA

^cFaculty of Education and Human Sciences, Niigata University, 8050 Igarashi 2 no cho, Niigata city, Niigata 950-2181, Japan

^dDepartment of Textile Technology and Product Development, China Textile Institute, No. 6, Chen-Tian Road, Tu-Chen City, Taipei Hsien, 236 Taiwan, ROC

Received 14 June 2004; received in revised form 10 November 2004; accepted 17 November 2004

Available online 15 January 2005

Abstract

Regenerated *Bombyx mori* silk fibroin in formic acid was electrospun and the morphological, chemical and mechanical properties of these nanofibers were examined by field emission environmental scanning electron microscopy (FESEM), Raman spectroscopy (RS), Fourier transform infrared (FTIR) spectroscopy, X-ray diffraction (XRD) and tensile testing. FESEM indicated that the average fiber diameter was less than 100 nm and circular in cross section. This paper maps the silk fibroin molecular conformations of each step of the sample preparation and the electrospinning process. The secondary structural compositions (random and β -sheet) of the fibroin were determined by FTIR and RS. The crystallinity index of the electrospun fiber, calculated as the intensity ratio of 1624 (β -sheet) and 1663 (random) cm^{-1} FTIR bands was higher than that of the pristine fiber. Raman spectra of the amide I (1665 cm^{-1} , random) to amide III (1228 cm^{-1} , β -sheet) ratio of the electrospun fiber was less than that of the pristine fiber indicative of higher β -sheet content. The fiber crystallinity, determined by XRD, showed a lower value for the electrospun fiber. The electrospun fiber shows small but significant increases in the β -sheet content in comparison with the pristine fiber. Dissolution of fibroin in formic acid enhances β -sheet crystallization and may facilitate β -sheet formation in electrospun fiber. The electrospun random silk mat had a Young's modulus, ultimate tensile strength and strain of 515 MPa, 7.25 MPa and 3.2%, respectively.

© 2004 Published by Elsevier Ltd.

Keywords: *Bombyx mori*; Electrospinning; Nanofibers

1. Introduction

1.1. Background

This is the third paper in a series of papers on the electrospinning of regenerated *Bombyx mori* silk. The initial paper studied the effect of electrospinning parameters on the morphology and fiber diameter and it was determined by statistical analysis that the silk solution concentration was the most important factor in producing uniform cylindrical fibers less than 100 nm in diameter [1]. The second paper utilized response surface methodology (RSM) to optimize

the electrospinning parameters to produce nanofibers. The RSM model showed that a concentration of 8–10% and an electric field of 4–5 kV/cm realized nanofibers of diameters less than 40 nm [2]. The silk source is an additional variable and each silk must be analyzed separately. In this paper, we study the effect of electrospinning process on the structure, morphology and properties of the silk fiber assemblies. The silk fibroin is characterized through the processing steps of degumming, dissolution in aqueous calcium chloride, dialysis, water removal, dissolution in formic acid and fiber formation. The compositional, structural and mechanical properties of the pristine and electrospun silk fiber assemblies are compared.

As described in the previous papers, electrospinning is an attractive method of producing nanoscale fibers from both

* Corresponding author. Tel.: +1 215 895 1640; fax: +1 215 895 6684.
E-mail address: fko@coe.drexel.edu (F. Ko).

natural [3,4] and synthetic polymers [5–8] with diameters ranging from 2 nm to several micrometers. Electrospinning can produce fibrous materials, which are comparable to or smaller in size than those of natural fibers including collagen, elastin and fibrinogen. Our laboratory has fabricated electrospun silkworm silk fibers with average diameters as low as 28 ± 15 nm.

The availability of silk nanofibers introduces a new set of potential uses that previously were unattainable. Silk nanofibers are attractive candidates for biomedical, electrical and textile applications, including tissue-engineered scaffolds, wound dressings and drug delivery systems [9–11] because of their high specific surface area, increased strength and surface energy and enhanced thermal and electrical conductivity.

Silk, a protein-based polymer with good biocompatibility and unique structural properties has long been used as a suture and textile material [12], in cosmetics and pharmaceuticals [13]. *Bombyx mori* silk fibers are 10–20 μm in diameter, appear triangular in cross section and consist of thousands of parallel fibrils, which give them their grainy surfaces. The fiber consists of an inner (fibroin) and outer layer (sericin) of protein. The triangular cross-section and the rough surface of the fiber may not be desirable for sutures because of possible abrasive damage to tissue. However, electrospinning regenerated silk fibroin, with sericin removed, produces circular-shaped fibers with improved biocompatibility. The anti-parallel β -pleated structure of silk is responsible for its strength and toughness [14,15].

These properties of silk and their potential benefits have generated an interest in electrospinning silk from various sources including silkworm cocoon [1,14,16,17], spider (*Nephila Clavipes*) dragline silk [17], recombinant hybrid silk-like polymers with fibronectin functionality [18] and a mixture of silk fibroin and chitin [19].

The electrospinning process of silk involves conformational changes in the silk fibroin from random coil to β -sheet and vice versa. An understanding of the structural changes that occur during the various stages of the electrospinning process is essential for the proper use of the regenerated silk for various applications.

2. Materials and method

2.1. Spinning dope preparation

The materials used in this study were purchased from Sigma-Aldrich. Degummed *Bombyx mori* silk fibers provided by the China Textile Institute in Taiwan, were dissolved in 50% aqueous CaCl_2 and dialyzed against deionized water. All concentrations were weight to weight (w/w). The dialyzed fibroin solution was frozen for 24 h at -20°C and then air-dried at room temperature. The

regenerated silk fibroin sponge was dissolved in formic acid (98–100%) to obtain 9–15% w/w concentrations.

2.2. Electrospinning

The critical electrospinning parameters (electric field and fibroin concentration) identified in part 1 of the paper series were optimized by a modified RSM method [2] employed in this study. Schematics of these experimental designs are shown in Fig. 1(A)–(C). The electric field ranged from 2–4 kV/cm and the concentration from 9 to 15%. Voltages of 10–50 kV and spinning distances of 5, 7 and 10 cm were

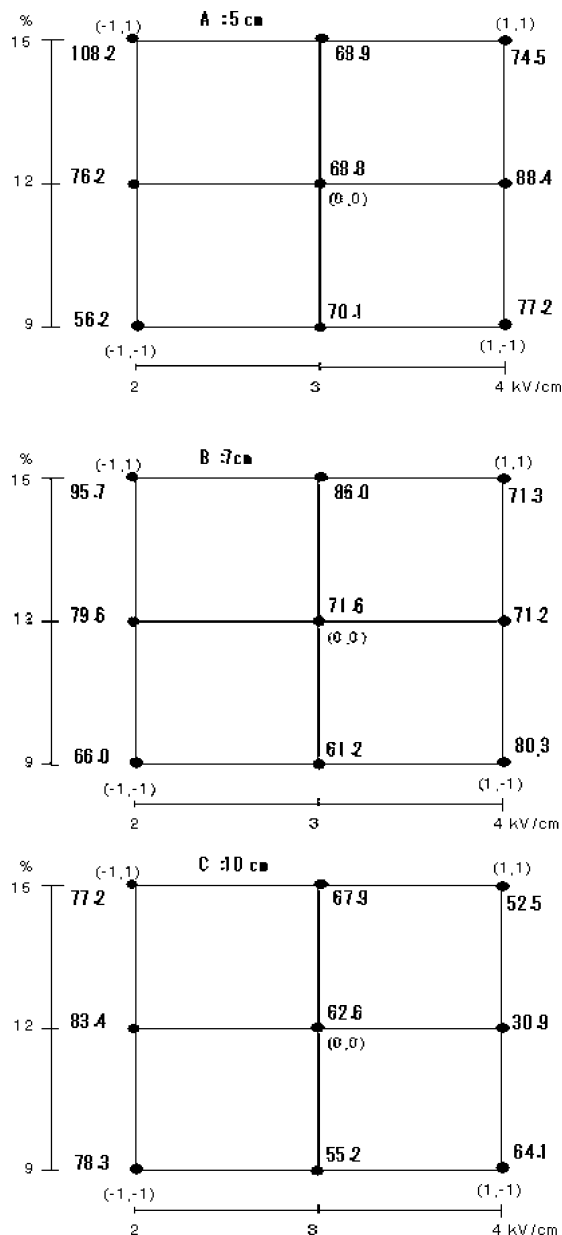


Fig. 1. Experimental design A: spinning distance 5 cm, B: spinning distance 7 cm and C: spinning distance 10 cm. The values at coordinate point show mean fiber diameter of 100 measurements and coded values are shown in the brackets (electric field, concentration).

utilized. The silk-formic acid dope was electrospun from an 18-G needle at a 45° spinning angle.

2.3. Characterization

The diameter of the gold-sputtered electrospun nanofibers were determined and examined by Phillips XL-30 FESEM. A measurement of 100 random fibers was used to determine average fiber diameter and distribution.

Raman Spectroscopy (Renishaw 1000–780 nm He–Ne diode laser), Fourier Transform Infrared Spectroscopy (FTIR-Nicolet Magna-IR 560 spectrometer) and wide angle X-ray diffraction (WAXD-Siemens D500) were used to elucidate the secondary structure, chemical composition and crystallinity of the silk fibroin at each stage of the electrospinning process.

The mechanical properties of the electrospun nonwoven mat were measured on the KES-G1 microtensile tester. The electrospun mat (after carefully removing the aluminum foil) was tested at room temperature (23 °C) and 65% humidity.

3. Results

3.1. Fiber morphology and diameter distribution

Concentration was found to be the most important parameter influencing the fiber diameter produced in the electrospinning process. For spinning distances of 5, 7 and 10 cm at low electric fields of 2–3 kV/cm, the fiber diameter was found to increase with an increase in fibroin concentration. A 9% fibroin concentration produced fibers with diameters ranging from 8 to 223 nm. A 15% fibroin concentration yielded fibers with diameters from 12 to 397 nm.

Fiber diameter distributions at a fibroin concentration of 9%, an electric field of 3 kV/cm and the three spinning distances are shown in Fig. 2(A)–(C). The average fiber diameters were 70 ± 23 , 61 ± 27 and 55 ± 26 nm at spinning distances of 5, 7 and 10 cm, respectively.

Fig. 3 shows the ESEM micrographs of electrospun fibers at spinning distance of 10 cm, electric field strength of 3 kV/cm and polymer concentrations of 9, 12 and 15 wt%. The fibers had smooth surfaces and appeared circular in cross-section (not shown in the Fig. 3).

3.2. Raman spectroscopy

The conformational changes of the secondary structure of silk fibroin, which occur during the electrospinning process, were analyzed by Raman spectroscopy.

The spectra for pristine, degummed and electrospun fibers are shown in Fig. 4(A). Pristine and degummed silk fibroins display characteristic conformational bands in the range 1650–1667 and 1241–1279 cm^{-1} which correspond

to amide I and complex amide III, respectively [20,21]. In this study, the amide I (random coil) pristine band was observed at 1665 cm^{-1} and the amide III (β -sheet) pristine band at 1231 cm^{-1} . These well-defined bands were chosen because they give a clear indication of changes in the secondary structures from random to β -sheet. The degummed silk also shows absorption bands at these wavelengths. No significant spectral changes were observed indicating that the fibroin conformation is unchanged during the degumming process. The Raman spectra of the electrospun fiber are essentially the same as that of the pristine and degummed fibers although minor bands and some differences in peak intensities appear. This shows that the electrospinning process preserves the natural conformation of the fibroin. Fig. 4(B) shows the amide I (1665 cm^{-1} , random) to amide III (1228 cm^{-1} , β -sheet) ratio of the electrospun fiber is less than that of the pristine fiber. This means that the electrospun fiber has a higher β -sheet content than the pristine fiber.

3.3. FTIR spectroscopy

The secondary structure of *Bombyx mori* silk fibroin consists of the major conformations including- random coils (silk I) and β -sheet (silk II) [22]. This paper does not differentiate between random coils and silk I structures because of their similar conformational structures [23]. FTIR spectroscopy was used to follow the conformational changes that occur during the electrospinning process. Random coils show strong absorption bands at 1665 (amide I), 1540 (amide II), and 1235 cm^{-1} (amide III) and the β -sheets show absorption bands at 1628 (amide I), 1533 (amide II) and 1265 cm^{-1} (amide III) [24].

Fig. 5(A) shows the FTIR spectra of degummed silk, silk fibroin (6% aqueous calcium chloride), silk fibroin (aqueous post dialysis) and silk fibroin (12% aqueous formic acid). There are no significant differences in the major peaks. This indicates that there are no significant conformational differences between the degummed fiber and the fibroin solutions.

Fig. 5(B) shows the FTIR spectra of pristine, degummed, dried fibroin sponge and electrospun silk fibers. There are no significant differences in the major bands. However, there are significant differences in peak intensities, which indicate changes in the secondary structure or concentration. The percent changes in the intensity of the 1663 cm^{-1} band (amide I, random) relative to the pristine silk are 0, 10 and 6 for the degummed fiber, dried fibroin sponge and electrospun silk mat, respectively.

The amide I crystallinity index, calculated as the intensity ratio of 1624 and 1663 cm^{-1} bands, is shown in Table 1 for each step of the electrospinning process. The amide I represents the most abundant secondary structure of fibroin and shows strong absorption bands at 1663 cm^{-1} (random) and 1624 cm^{-1} (β -sheet). Fig. 5(C) shows the qualitative values of the crystallinity index indicative of

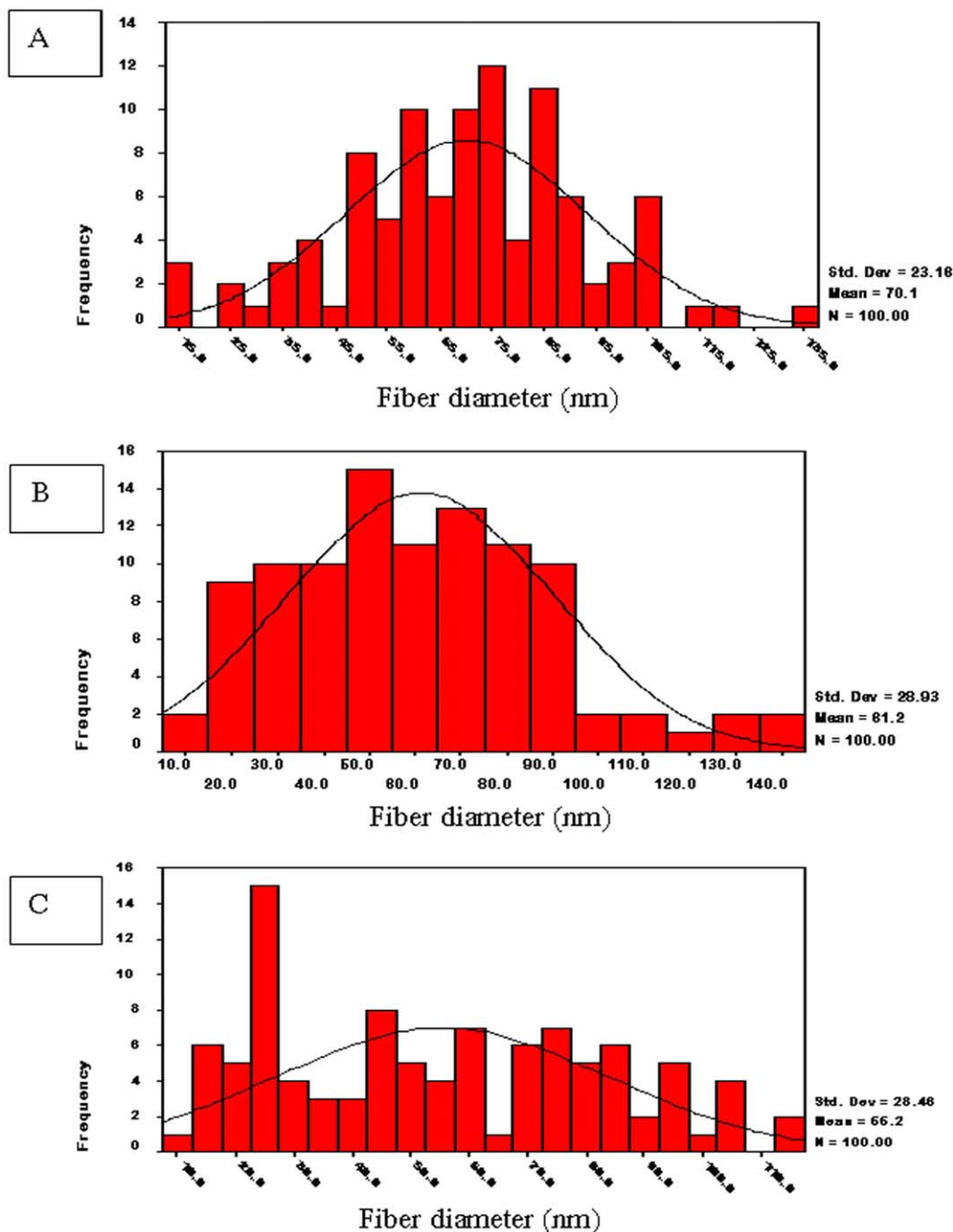


Fig. 2. Fiber diameter distribution: (A) for 9% silk, 5 cm spinning distance and electric field of 3 kV/cm, (B) for 9% silk, 7 cm spinning distance and electric field of 3 kV/cm and (C) for 9% silk, 10 cm spinning distance and electric field of 3 kV/cm.

secondary structure changes. These results indicate an increase in the β -sheet of the electrospun nanofiber in comparison with the pristine and degummed fibers.

3.4. Structural analysis by wide angle X-ray diffraction (WAXD)

WAXD was used to determine the crystalline structure of the fibroin. Fig. 6 shows the WAXD patterns of pristine and electrospun fibers. The similarities between the patterns of

the two systems strongly suggest structural similarity between the pristine and electrospun fibers. The pristine fiber was characterized by the presence of five diffraction peaks at 13.7, 16.5, 18.2, 25.3 and 28.1°, corresponding to silk (I) and silk (II) crystalline d spacings of 6.5, 5.4 (II), 4.9 (II), 3.5 (I), 3.2 (I) Å, respectively. The electrospun fiber was characterized by diffraction peaks at 13.7, 16.6, 18.3, 25.4 and 28.6°, corresponding to silk (I) and silk (II) crystalline d -spacings of 6.5, 5.3 (II), 4.8 (II), 3.5 (I) and 3.1 (I) Å, respectively. Within experimental error, these results

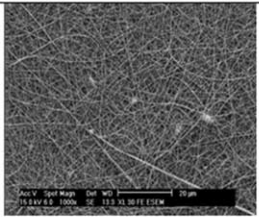
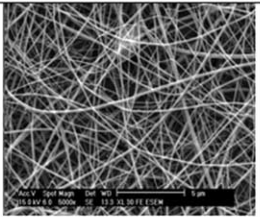
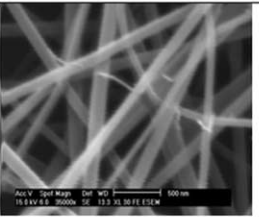
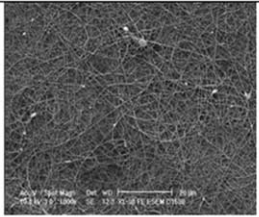
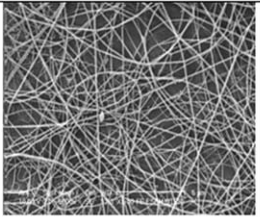
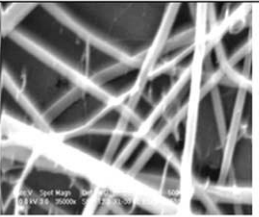
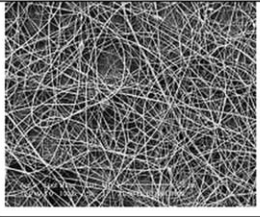
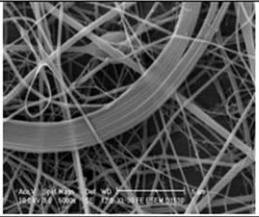
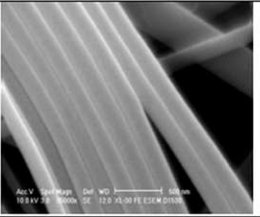
| 10cm,3kv | Magnification | | | Fiber diameter (nm) |
|----------|---|---|--|---|
| | 1000x | 5000x | 35000x | |
| 9% |  |  |  | AV: 55.2 STDV: 28.5 Max: 117.0 Min: 7.8 |
| 12% |  |  |  | AV: 62.6 STDV: 32.9 Max: 175.8 Min: 14.9 |
| 15% |  |  |  | AV: 98.6 STDV: 58.4 Max: 212.7 Min: 15.6 |

Fig. 3. ESEM micrographs of electrospun silkworm silk fibers and their corresponding processing parameters of electric field of 3 kV/cm, spinning distance of 10 cm and concentrations of 9, 12 and 15%, respectively.

are in agreement with the findings of Asakura [23], Hayakawa [25] and Jin [26]. The diffraction patterns indicate preferred orientation of the molecular axis of the crystals along the fiber axis. The results show that both types of fibers are comprised of mixtures of random (silk (I)) and β -sheet (silk (II)) crystals, i.e. none of the fibers consist of only one type of crystal. The unknown d-spacing value of 6.5 may be due to other types of conformations such as helical and β -turns or distortions by the presence of conformers and/or segments in which torsion angles deviate from those of random or β -sheet. The crystallinity of the fibers was calculated by the method of Herman [27]. The

crystallinity of the pristine and electrospun fibers was 48 and 39%, respectively.

3.5. Mechanical analysis by tensile testing

The mechanical properties of the electrospun random fiber mats were determined utilizing a Kawabata KES-G1 microtensile tester. Strips measuring 0.5 by 4 cm were mounted on paper sample holders (3 cm gauge length). A strain rate of 0.02/s, sensitivity setting of 5 and frequencies of 50 Hz were used in the tensile tests. The results of the experiment were computed in load (gram force) vs. displacement. The specific stress in gm/Text was then calculated using the following equation:

$$\text{Stress (gm/Text)} = \frac{\text{Force (gm)/specimen width (mm)}}{\text{Areal density (gm/m}^2\text{)}}$$

The areal density is simply the weight (gm) of the nonwoven silk test strip divided by the area of the test specimen. The stress in gm/Text was converted to N/Text by multiplying it by 0.0098. This was converted into the stress in GPa by multiplying it by the density of silk, taken as 1.25 gm/cc. The conversion factor is shown in the equation below:

$$\text{Stress (MPa)} = \text{Stress (gm/Text)} \times 0.81633$$

The strain was calculated by dividing the displacement by the gauge length.

Table 1
Crystallinity index of silk fibroin determined for each step of the electrospinning process

| Amide | |
|------------------------------|---------------------------|
| Type of silk | Peak ratio (1624/1663), % |
| Pristine | 48.8 |
| Degummed | 48.8 |
| Fibroin in CaCl ₂ | 49.5 |
| Fibroin after dialysis | 48.2 |
| Dried sponge | 48.7 |
| Fibroin in formic acid | 49.0 |
| Electrospun silk mat | 50.2 |

The index is calculated from the amide I peak intensities at 1624 and 1663 cm⁻¹. The indices were not significantly different based on the two way ANOVA test carried out at the confidence interval of 95%.

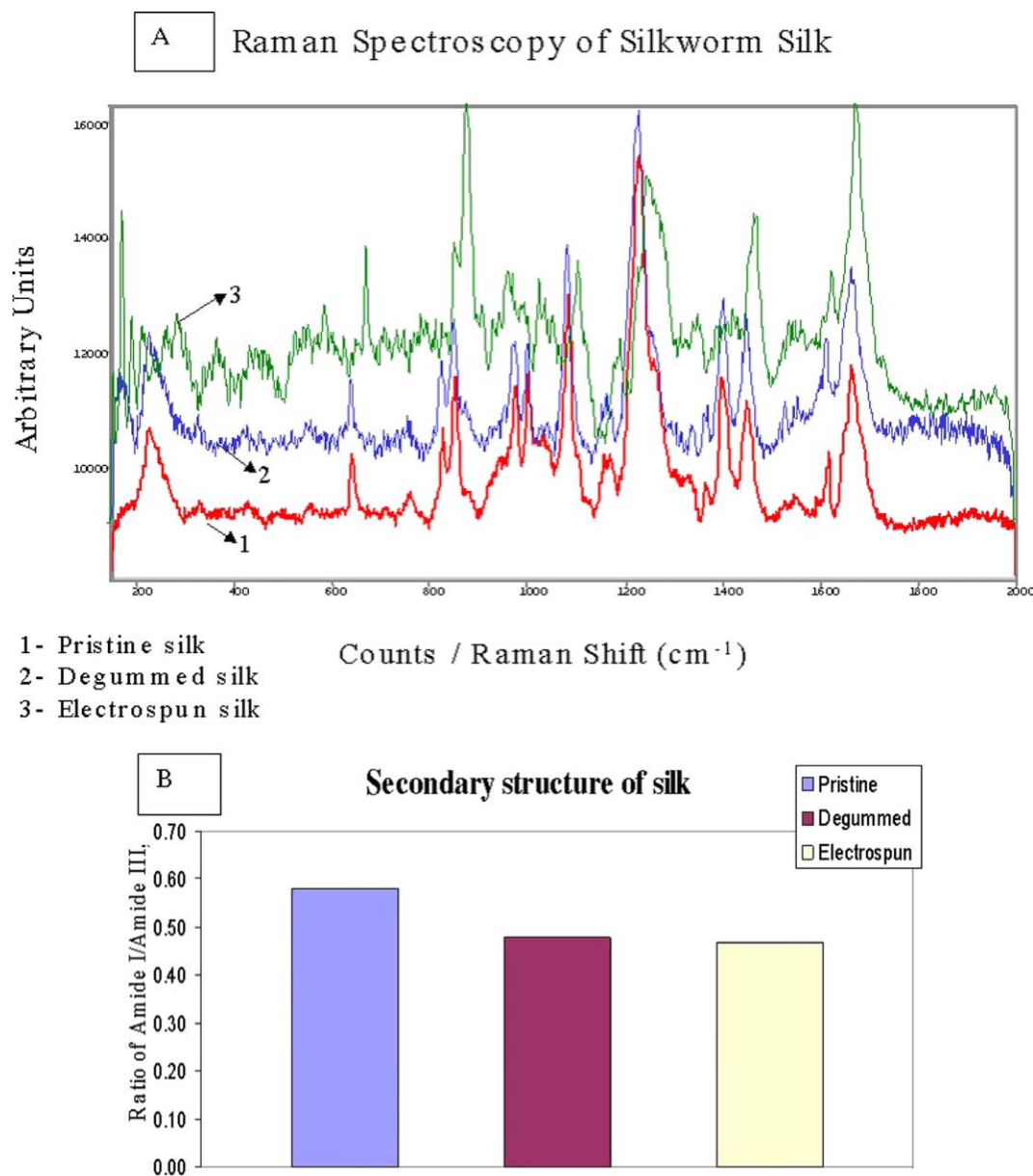


Fig. 4. (A) Raman spectroscopy of pristine, degummed and electrospun nonwoven silk mat. (B) Secondary structural compositions of silk fibroin showing the fraction of Amide I to Amide III conformations.

Fig. 7 shows the preliminary result of the mechanical tests. The initial part of this curve shows a high resistance to deformation due to cohesive forces in the fiber assembly as a result of the large number of fiber-to-fiber contacts that is a consequence of the nanoscale fiber diameter. A pseudo-yield point is also observed after the initial linear portion of the stress-strain curve followed by a gradual reduction in modulus caused by the initiation of fiber slippage. The fiber slippage leads to slight fiber alignment along the tensile axis that results in a slow increase in stresses being generated. Further increases in strain (stretching) lead to decreases in the cross section of the test specimen and thus the number of fibers in the cross-section resulting in failure of the fiber assembly.

The initial modulus of the electrospun random mat as calculated from the slope of the initial part of the stress-strain curve was 515 MPa. The breaking strain and ultimate tensile strength of the fiber mat were 0.032 and 7.25 MPa, respectively. This compares quite favorably to the results obtained in an earlier study by Yang et al., wherein a breaking strain of 0.014 and a modulus of 1.29 MPa was observed for spun-bonded natural silk nonwoven fabrics [28]. An observation of the deformation mechanism of the nonwoven mat revealed nano-level drawing in some of the fibers as shown in Fig. 8. This implies that the molecular structures of the fibers can be further oriented. The fact that not all the fibers experienced the same drawing effect suggests that mechanical properties of the silk have not been

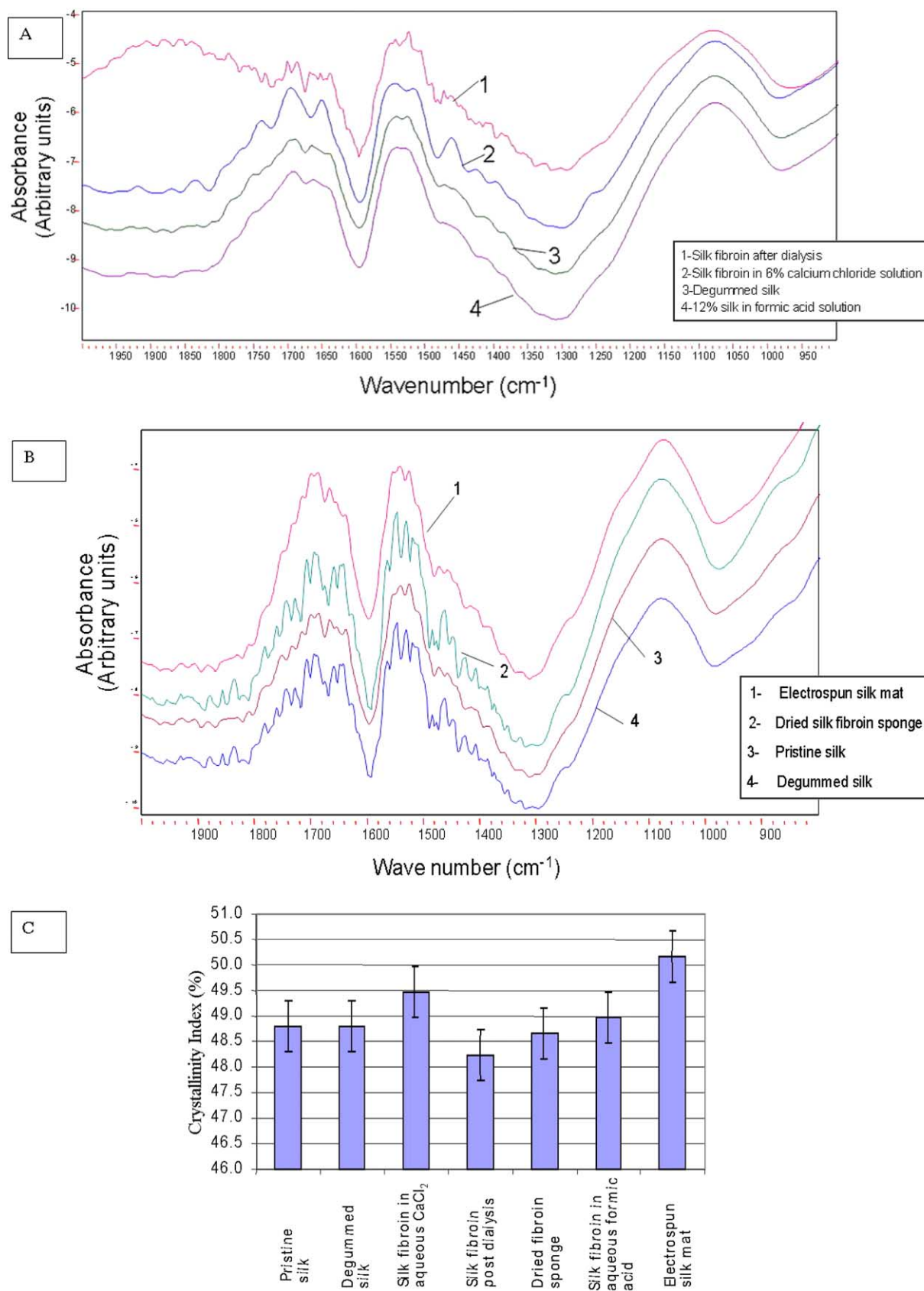


Fig. 5. (A) The FTIR spectra of—(1) dialyzed silk fibroin in water, (2) 6% silk fibroin in calcium chloride solution, (3) degummed silk fiber, (4) 12% silk fibroin in formic acid. (B) The FTIR spectra of—(1) electrospun silk mat, (2) dried silk sponge, (3) pristine and (4) degummed silk. (C) Crystallinity index of silk fibroin at each step of the electrospinning process.

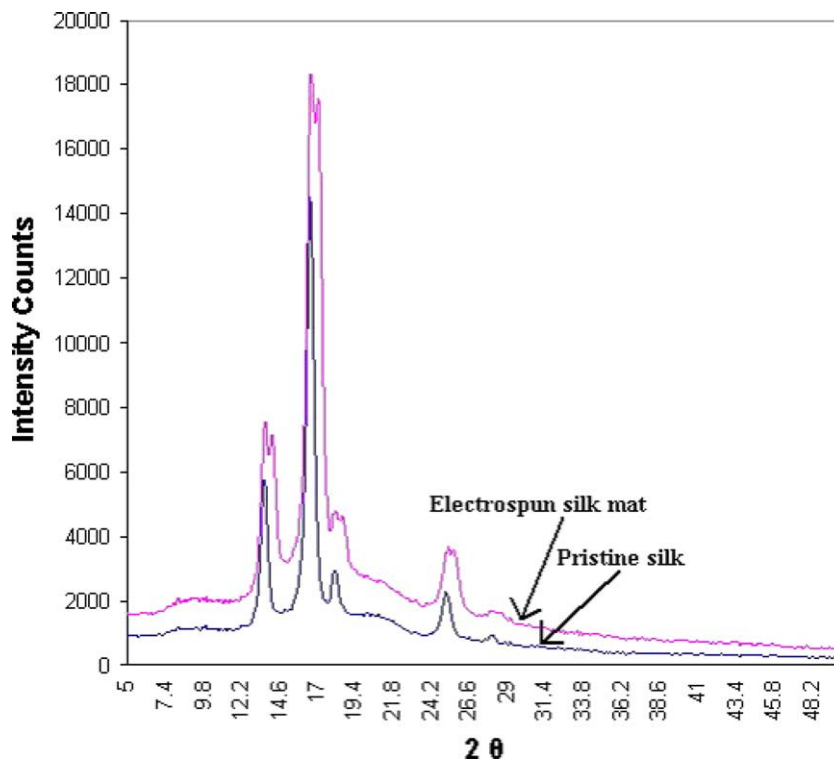


Fig. 6. WAXD of pristine and electrospun silk fibers.

fully realized. According to the mechanics of nonwoven fabrics [29], the theoretical Young's modulus of a fiber (E_f) can be estimated as a first approximation to be 1.37 GPa from the modulus of a nonwoven fabric (E_F) as follows:

$$E_f = 8/3 E_F$$

This value is an order smaller than that of natural silk fibers, e.g. the modulus and ultimate tensile strength of *Bombyx mori* silk fiber is 16 GPa and 650 MPa, respectively. Further alignment of silk fibers and proper drawing of the aligned fiber assemblies will be necessary in order to attain the required mechanical properties of the nanofibers.

4. Discussion

Bombyx mori fibroin is comprised of dimorphic structures (random coil and β -sheet), which can easily be interconverted during fibroin processing. In this study the conformational changes, i.e. transition between random coil and β -sheet were evaluated at each step of the electrospinning process. The mechanical properties of the electrospun silk mat were also determined.

The relative amounts of the random coil and β -sheet structures were measured by FTIR. The FTIR shows that there are no conformational changes in the relative amounts of random and β -sheet contents of the pristine and degummed fibers. Dissolution in calcium chloride leads to conversion of random structure into β -sheet as shown by an

increase in the crystallinity index of dissolved fibroin. The crystallinity indexes of degummed fibroin and fibroin dissolved in calcium chloride are 48.8 and 49.5%, respectively as shown in Fig. 5(C). This agrees with studies that show cations such as Ca^{2+} , Na^+ and K^+ in the fibroin solution facilitate the transition of random coil to β -sheet [30]. Conversely, removal of Ca^{2+} cation reverses the conformational transition. This is consistent with our observation of the dialyzed fibroin that has a lower index of 48.2%. The aqueous environment also favors the transition of β -sheets into random coils. The index increases slightly during the drying process to produce a sponge due to an increase in intramolecular hydrogen bonding of the fibroin.

Dissolution of fibroin in formic acid increased the crystallinity index to a greater extent than dissolution in water, which is consistent with the observation of Um et al. [24]. They reported that formic acid promotes the β -sheet crystallization, therefore reducing the hydrodynamic radius of the fibroin molecules and increasing intramolecular hydrogen bonding of the fibroin. Um also noted that removal of formic acid from the fibroin leads to a further increase in the β -sheet content. Elimination of formic acid during the electrospinning process produces nanofibers with a crystallinity index of 50.2%, the highest observed. The electrospinning process also promotes fibroin molecular alignment [31], enhancing crystallization.

The Raman results also indicate that there are no significant conformational differences between the pristine,

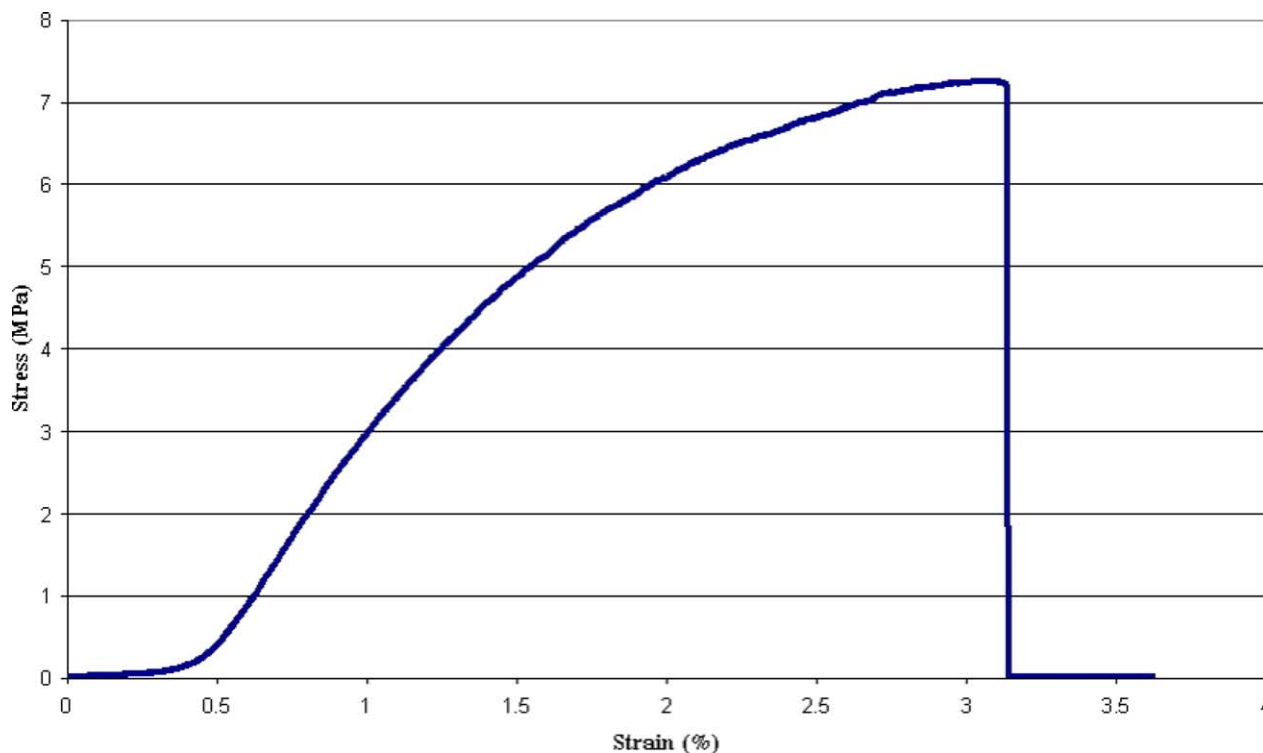


Fig. 7. Stress–strain curve of electrospun random silk mat (concentration of 15%, electric field of 2 kV/cm and 5 cm spinning distance).

degummed and electrospun fibers. A decrease in the relative amounts of amide I/amide III of the electrospun fiber in comparison with the pristine fiber is an indication of an increase in β -sheet content. This is consistent with the FTIR result that also shows an increase in β -sheet content.

The WAXD results compliment the findings by Raman and FTIR regarding the crystalline structure of the electrospun silk fiber in comparison with the pristine sample. The pristine and electrospun fibers are both comprised of mixtures of random (silk (I)) and β -sheet (silk (II)) crystals. The crystallinity of the pristine and

electrospun fibers was 48 and 39%, respectively. These results show that the electrospun fibers are crystalline in nature which is contrary to earlier reports [17,33] of the fibers being amorphous. This is probably due to the use of formic acid as a solvent in our study which induces long range ordered crystallites.

The discrepancies in the value of the crystallinity (WAXD) and crystallinity index (FTIR) are due to the difference in the detecting method employed. FTIR is sensitive to short-range ordered structures and WAXD is sensitive to long-range ordered structures [32].

The modulus of the electrospun random silk mat as determined by the mechanical tests was 515 MPa with a breaking strain of 0.032. These values are lower than that of natural silk fibers because of fiber slippage caused by frictional forces between fibers during testing. A more accurate analysis can be achieved by testing aligned fibers. Further drawing and annealing would also increase the mechanical properties of the fibers.

5. Conclusion

In order to understand the structural changes caused by the processing steps in the electrospinning process, the conformational transitions from random coil to β -sheet characterized by the crystallinity index was determined by FTIR and the relative amounts of amide I to amide III by RS. The conformational changes that occur during the

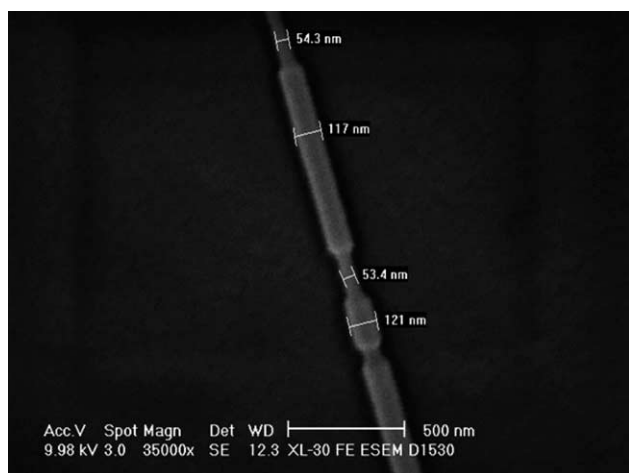


Fig. 8. ESEM of electrospun nanofiber after mechanical tensile testing showing nano-drawing effect.

various processing steps prior to and during the electrospinning process are as follows:

- Degummed fibroin: the crystallinity index of the pristine and degummed fibers was the same. Degumming does not alter the secondary structure of the silk fibroin.
- Dissolution in calcium chloride: the crystallinity index of the silk from the fibroin solution was higher than degummed fiber indicating that calcium ion facilitates the formation of β -sheet.
- Dialyzed fibroin: removal of calcium ion causes a decrease in crystallinity index. The aqueous environment also facilitates the transition to random structure.
- Dried fibroin sponge: removal of water leads to a slight increase in the crystallinity index due to an increase in intermolecular hydrogen bonding of the fibroin.
- Dissolution in formic acid: formic acid increases the β -sheet crystallization and reduces the hydrodynamic radius of the fibroin molecules by increasing intramolecular hydrogen bonding of the fibroin.
- Electrospun fibers: the removal of formic acid and the fibroin molecular alignment, which occurs during electrospinning result in the highest observed crystallinity index.

The results of this study show that the electrospun fiber has a non-negligible increase in the β -sheet content in comparison with the pristine fiber. Dissolution of fibroin in formic acid enhances β -sheet crystallization and may facilitate β -sheet formation in the electrospun fiber. However, the mechanical properties of the electrospun fiber are not fully realized due to misorientation on the molecular and fibril level. Further study will be carried out using aligned electrospun fibers and post processing treatments such as fiber drawing, annealing and methanol treatment to improve on the mechanical properties.

Acknowledgements

Funding for this project was provided by China Textile Institute, Taiwan, ROC. The authors greatly appreciate the support provided to Sachiko Sukigara by the Ministry of Education, Culture, Sports, Science and Technology through Niigata University in Japan. This project is supported in part by the PA Nanotechnology Institute. We thank David Von Rohr and Tim Kelly for their experimental assistance. The instruments used in this work are operated by the Department of Materials Engineering at Drexel University. The Raman spectrometer and FESEM purchase were supported by the NSF (DMR-0116645) and NSF (BES-0216343), respectively.

References

- [1] Sukigara S, Gandhi M, Ayutsede J, Micklus M, Ko F. *Polymer* 2003; 44:5721–7.
- [2] Sukigara S, Gandhi M, Ayutsede J, Micklus M, Ko F. *Polymer* 2004; 45(11):3701–8.
- [3] Fang X, Reneker DH. *J Macromol Sci, Phys* 1997;36(2B):169.
- [4] Matthews JA, Wnek GE, Simpson DG, Bowlin GL. *Biomacromolecules* 2002;3(2):232–8.
- [5] Doshi J, Reneker DH. *J Electrostat* 1995;35:151–60.
- [6] Jin HJ, Fridrikh SV, Rutledge GC, Kaplan DL. *Biomacromolecules* 2002;3:1233–9.
- [7] Li WJ, Laurencin CT, Catterson EJ, Tuan RS, Ko F. *J Biomed Mater Res* 2002;4:613–21.
- [8] Zong X, Kim K, Fang D, Ran S, Hsiao BS, Chu B. *Polymer* 2002;43: 4403–12.
- [9] Huang ZM, Zhang YZ, Kotaki M, Ramakrishna S. *Compos Sci Technol* 2003;63:2223–53.
- [10] Zeng J, Xu X, Chen X, Liang Q, Bian X, Yang L, Jing X. *J Controlled Release* 2003;92:227–31.
- [11] Kenawy ER, Bowlin GL, Wnek GE. *J Controlled Release* 2002;81: 57–64.
- [12] Ogho K, Zhao C, Kobayashi M, Asakura T. *Polymer* 2003;44:841–6.
- [13] Brooks G. *Drug Cosmet Ind* 1989;145(4):32–6.
- [14] Altman GH, Diaz F, Jakuba C, Calabro T, Horan RL, Chen J, Lu H, Richmond J, Kaplan DL. *Biomaterials* 2003;24:401–16.
- [15] Panilaitis B, Altman GH, Chen J, Jin HJ, Karageorgiou V, Kaplan DL. *Biomaterials* 2003;24(18):3079–85.
- [16] Kim SH, Nam YS, Lee TS, Park WH. *Polym J* 2003;35(2):185–90.
- [17] Zarkoob S, Reneker DH, Eby RK, Hudson SD, Ertley D, Adams WW. *Polym Preprints* 1998;39(2):244–5.
- [18] Buchko CJ, Chen LC, Shen Y, Marthin DC. *Polymer* 1999;40: 7397–407.
- [19] Weixan L. *J Textile Res* 2003;24(5):80–2.
- [20] Zhou L, Chen X, Shao Z, Zhou P, Knight DP, Vollrath F. *Fed Eur Biochem Soc Lett* 2003;554:337–41.
- [21] Monti P, Freddi G, Bertoluzza A, Kasai N, Tsukada M. *J Raman Spectrosc* 1998;29(4):297–304.
- [22] Chen X, Shao Z, Marinkovic NS, Miller LM, Zhou P, Chance MR. *Biophys Chem* 2001;89(1):25–34.
- [23] Asakura T, Kuzuhara A, Tabeta R, Saito H. *Macromolecules* 1985;18: 1841–5.
- [24] Um IC, Kweon HY, Lee KG, Park YH. *Int Biol Macromol* 2003;33: 203–13.
- [25] Hayakawa T, Kondo Y, Yamamoto H, Noguchi J. In: Nobumasa H, editor. *Structure of silk yarn, part b: chemical structure and processing of silk yarn*. Enfield, NH: Science Publishers; 2000. p. 87–104.
- [26] Jin HJ, Kaplan DL. *Nature* 2003;424:1057–61.
- [27] Weidinger A, Hermans PH. *Die Makromolekulare Chemie* 1961;50: 98–115.
- [28] Yang R, Fang P, Ko F. In: Kawabata S, Postle R, Niwa M, editors. *Evaluation of the hand of spun bonded silk in objective measurement: applications to product design and process control*. Japan: The Textile Machinery Society of Japan; 1986. p. 547–56.
- [29] Gutowski TG, editor. *Advanced composite manufacturing*. Wiley; 1997. p. 17–18.
- [30] Zhou L, Chen X, Shao Z, Zhou P, Knight DP, Vollrath F. *Fed Eur Biochem Soc Lett* 2003;554:337–41.
- [31] Anderson JP, McGrath K, Kaplan D, editors. *Protein-based materials*. Basel: Birkhauser; 1997. p. 371–423.
- [32] Um IC, Kweon HY, Park YH, Hudson S. *Int J Biol Macromol* 2001; 29:91–7.
- [33] Wang M, Jin HJ, Kaplan DL, Rutledge GC. *Macromolecules* 2004; 37(18):6856–64.